Impact of Precipitation Parameters on the Specific Surface Area of PuO$_2$

Eric Hoar*, Thomas C. Shehee and Lindsay E. Roy

Contributions from Savannah River National Laboratory, P. O. Box A, Aiken, SC 29808

[*] To whom correspondence should be addressed (eric.hoar@srnl.doe.gov)

Abstract

Controlling the properties of PuO_2 through processing is of vital importance to environmental transport and fate, production of nuclear fuels, nuclear forensic analyses, stockpile stewardship, and storage of nuclear wastes applications. A number of processing conditions have been identified to control final product properties, including specific surface area (SSA), residual carbon content, adsorption of volatile species, morphology, and particle size. In this paper, a novel approach is developed for the prediction of PuO_2 SSA via the synthetic route of Pu(IV) oxalate precipitation followed by calcination. The proposed model utilizes multivariate regression methodology and leave one out (LOO) formalism to link Savannah River Site (SRS) precipitation and calcination production data to the SSA of the final product. A comparison among the models provides insight into the accuracy and ability to identify variations amongst the processing data. Additionally, the models may also be used to fit new data outside of the parameters explored in a production facility. Finally, the trained model was compared to a similarly trained conventional model form to illustrate the influence of precipitation parameters on the prediction of the final SSA. The models presented here attempt to provide new methods for more accurate prediction of the PuO_2 product properties in a production scale environment for key environmental and nuclear applications.

Introduction

For decades plutonium(IV) oxide has been studied in both laboratory and industrial scale settings to understand how the physical characteristics and chemical stability are controlled by changes in process parameters of the production process.[1-7] Several dependencies have been linked to the different chemical preparation routes, e.g. peroxide, oxalate, hydroxide precipitation or metal oxidation. However, the most commonly studied synthetic route via Pu(III/IV) oxalate intermediate precipitation produces diverse final oxide characteristics depending on the processing conditions.[8] In general, the mean particle size, shape, and morphology are controlled by the precipitation process parameters whereas the specific surface area (SSA), tap density, residual moisture content and carbon content are functions of the calcination process.[1,9] While these are the dominant processing conditions affecting the final oxide product, insights into the interplay between the two remain incomplete due to the wide parameter space among the processing units. For example, a variance in the SSA of 5-15 m^2/g is seen at a calcination temperature of 650°C, with wider window occurring at lower calcination temperatures. Indeed, when analyzing processing conditions outside of comparing calcination temperature to the SSA specifically, it appears that no dependency exists in either the literature or using known data.[2,3,8-10]

Recent work which explored process dependencies between the PuO$_2$ product characteristics and the preparation method has analyzed the effect of adding calcination time to known temperature data to produce a complex correlation using the two variables.[1,2] The data were curve fit using a non-linear regression function over a wide temperature range and suggested a time dependency with the SSA around 2.5-3 hrs. A subset of the data was further analyzed using a narrower temperature range more in-line with industrial-scale processing parameters and showed minimal dependence on the time to predict the SSA. Orr *et al.* then developed an exponential function to fit known experimental SSA data based on temperature alone with 95% predictive accuracy.[1] However, the SSA distribution is still wide especially at temperatures below 650°C, suggesting that additional process-dependent conditions could exist and be traced to the final PuO$_2$ product. In other words, perhaps there are unidentified interdependencies that can be extracted beyond evaluating processing conditions associated with one unit operation (such as calcination).

Since our basic premise is that other processing parameters may account for variability in the SSA within a small calcination temperature window, we turned to data-driven regression modeling as a starting point for analysis. Although less accurate compared to machine learning models, data-driven regression models provide an interpretability not available with some machine learning algorithms.[11] Furthermore, data-driven regression models utilize some amount of domain knowledge in their creation because the parameters tend to be defined in physical terms versus machine learning models.[12,13] Due to this interpretability, it is possible to use data-driven models to see the influence of individual parameters by comparing their associated weighting values. The largest difference between the two model types exists in the amount of training data required to obtain an accurate prediction. For good machine learning algorithms, the minimum amount of

training data required can vary from hundreds to thousands of data points while for more simple regression models only require tens of data.[14] It can be easily stated that the required minimum amount of training data will change based on application, scope and/or modeling algorithm. Ultimately though, the trend that more data lead to a more accurate model exists for both model types.

Herein, we develop a data-driven model capable of utilizing PuO_2 processing parameters to predict the SSA. Our particular interest is to evaluate industrial-scale processing data during the precipitation and calcination of Pu(IV) oxalate, since the correlation may be more complex than at the laboratory scale. Results suggest that while the PuO_2 SSA is strongly correlated to the calcination processing conditions, other parameters can cause variations in the SSA from the value predicted using the conventional quasi-exponential temperature model. These variations can provide insight into the large variability of SSA at a small calcination temperature window thus increasing the predictive capability of calcination models.

Motivation and Methodology

From 2014-2018, a mission at SRS was to process plutonium metal to produce PuO_2 for feed to the MOX Fuel Fabrication Facility (MFFF) with a targeted production rate of 1 metric ton per yr.[15,16] The flowsheet proceeded as follows: After dissolution of Pu metal in 8 M nitric acid, the solution was then purified via anion exchange, precipitated as Pu(IV) oxalate, and calcined at ~650°C for at least 4.5 hrs to form PuO_2. The Pu(IV) oxalate was precipitated using the direct strike batch method, or adding 0.9 M oxalic acid to a Pu(IV) nitrate solution at 55 °C. An excess of 0.1 M oxalic acid and target nitric acid concentration between 1.5-3 M was necessary to minimize Pu losses and to produce a more dense PuO_2 product.[15,16] In addition to tracking trace element impurities throughout the process, the physical characteristics of the oxide powders, such as bulk and tap density, SSA, particle size, and moisture content were also measured. Table 1 shows the range of each processing parameter explored in this study, specifically the target nitric acid and Pu(IV) nitrate concentrations during precipitation, and the calcination temperature and time. The SSA range during the PuO_2 production campaign was 4-11 m^2/g. It is important to note that other processing variables were also analyzed (e.g. agitation time, cake mass, air flow), but these 4 parameters were found to be most relevant when correlating the SSA to the processing conditions (see below). Also, several parameters remained constant during the process and while they could have an effect (e.g. oxalic acid concentration, agitation rate), there was not enough variability in the data to draw conclusions at this time.

Table 1. Range of processing parameters at SRS during the PuO_2 production campaign used in this study.

Parameter	Minimum Value	Maximum Value
Nitric Acid Concentration (M)	1.7	2.7

Pu(IV) Nitrate Concentration (g/L)	25	45
Calcination Temperature (°C)	655	695
Calcination Time (min)	275	655

Several studies have analyzed the SSA of the final PuO_2 product with respect to the calcination temperature because of its importance in understanding radiolytic decomposition of water on the PuO_2 surface.[1-4,17-26] Since the 1960s, the quasi-exponential decrease in the SSA as a function of increasing calcination temperature is thought to be the result of crystalline rearrangement occurring at high temperatures, leading to the disappearance of pores and irregularities on the surface. [1-4] A plot of the SRS SSA vs. calcination temperature data (**Figure 1**) illustrates that an exponential relationship does not describe the trend over a narrow temperature range. Another interesting observation, higher calcining temperatures in general led to higher SSA in the dataset, which is counterintuitive to higher temperatures leading to decreasing surface areas. During production runs, two furnaces were used, one calcining at ~665°C and the other at ~690°C. In many cases, the time required to heat the oxalate product in the lower temperature furnace to the set temperature exceeded the facility threshold requirements, thereby necessitating an additional ~4.5 hrs of calcination time.
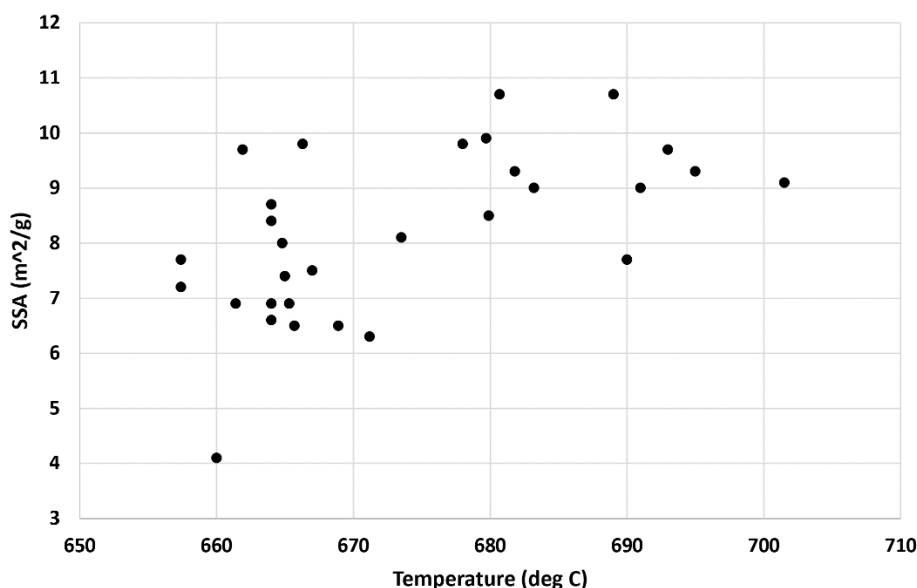

Figure 1: Comparison of SSA vs calcination temperature for all SRS data.

Preliminary investigation of the SRS data showed an interesting relationship between the nitric acid molarity and SSA not previously identified in the literature. This subset represents data where variation occurred only in the nitric acid concentration; the Pu concentration, calcination temperature, calcination time, and cake size remained near constant. **Figure 2** shows that the effect of the nitric acid molarity on the SSA can be characterized by a negative linear correlation. This

newfound result acted as the basis for analyzing several different process parameters for potential correlations to the PuO_2 physical characteristics, which were ultimately narrowed down to the nitric acid molarity, Pu(IV) nitrate concentration, and calcination temperature and time.
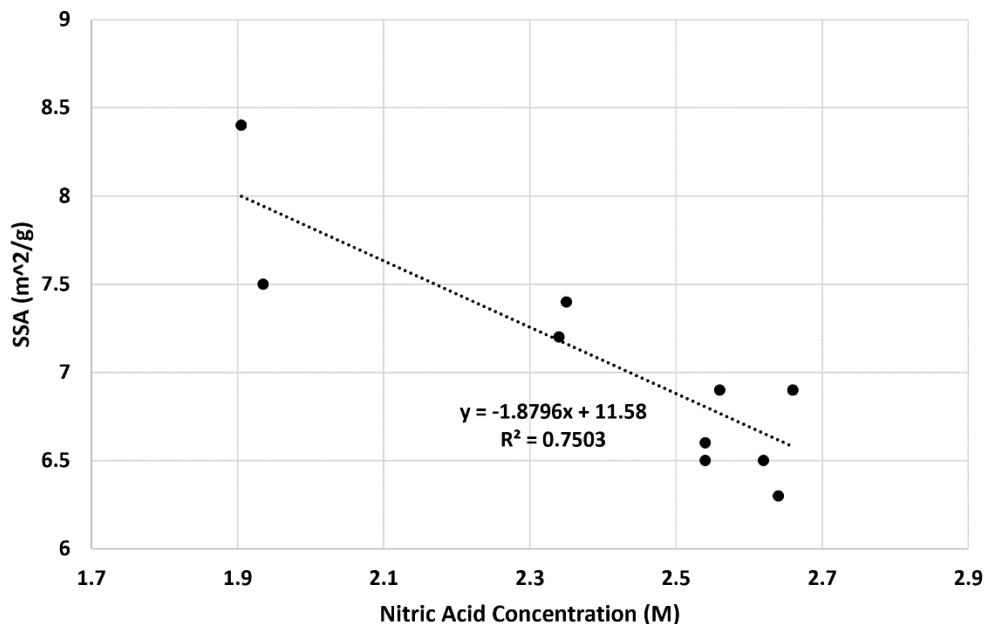

Figure 2: Effect of nitric acid molarity on SSA based on a subset of the SRS PuO_2 data. Trend line corresponds to the equation $y = -1.8796x + 11.58$ and had a R^2 value of 0.7503.

Of the 39 batch runs, our analysis only considered 27 as the others were identified as outliers falling outside normal processing conditions; SSA range for those data is 6-11 m^2/g. The resultant SRS dataset was further divided into training and testing sets using an iterative leave-one-out (LOO) approach[27] to provide an unbiased identification of a model's performance. **Figure 3** describes a flowchart of the iterative LOO approach utilized here.
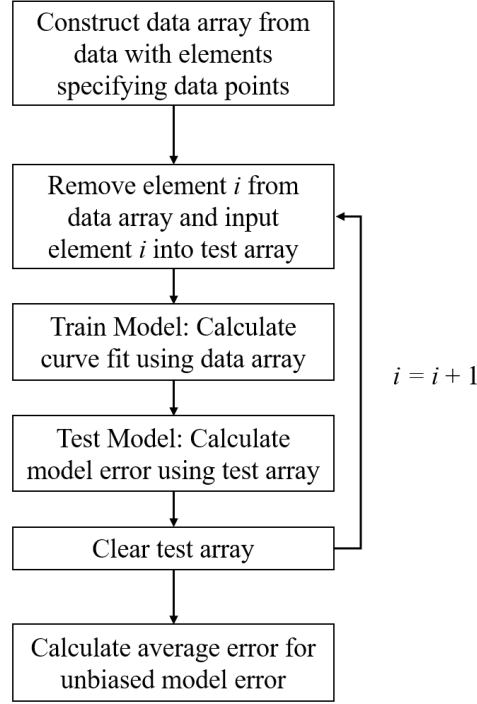
Figure 3: Flowchart of the iterative leave-one-out methodology. The loop is repeated until i is equal to the number of data points in the data array.

In this paper, 26 data points acted as the training data and 1 data point for the testing dataset, wherein the model was iterated resulting in total 27 different models. After each training and testing stage, the testing data point was changed and the model was reanalyzed utilizing the new data sets. This was repeated until each data point was utilized as a testing data point. This methodology provides an avenue for identifying the true capabilities of the model without bias as some data points would result in high error being very different from the training data set while other data points would result in low error being very similar to the training data set. The training data set was used to train a linear multi-variable model to predict the SSA after calcination. Equation 1 shows the generalized form of the where the variables, A_n, correspond to the weighting values which will be calculated using the training data set.

$$A_1 * T + A_2 * t + A_3 * M + A_4 * C = SSA \tag{1}$$

Equation 1 was fit for three independent model forms each utilizing different processing input parameters. The first form analyzes the calcination temperature (**T**) and time (**t**) as the variable of interest (i.e. $A_3 = A_4 = 0$). The second form examines relationship between the nitric acid (**M**) and Pu(IV) nitrate (**C**) concentrations only as a model variable (i.e. $A_1 = A_2 = 0$). The final model form utilizes all four process parameters of interest to illustrate if remnant precipitation conditions have bearing on the material properties after calcination. Comparison of the four process parameters and the yield confirms that the process parameters are not intercorrelated, and thus multicollinearity is avoided (Figure S1 in supplementary material). This final model form

attempts to provide information on processing history to more accurately model product characteristics. Finally, statistical analyses were performed on each of the model forms to illustrate the predictability of each form.

Results and Discussion

Initial evaluation of the PuO$_2$ SSA with the processing data considered only calcination temperature and those results are described in the supplementary material. Using a linear relationship, the average SSA among all the runs is 8.292 m^2/g with an average error of 14%. Because the temperature-only prediction to experiment is fairly vertical, and the data range between 6-11 m^2/g over a small temperature window, our next consideration added calcination time to the model since roughly half of the process runs included an extended calcination period. Equation 2 describes the simplified forms of Equation 1 for the prediction of SSA using this new model form with the coefficients of A_1 and A_2 being 0.0142 and -0.00235, respectively.

$$0.0142 * \boldsymbol{T} - 0.00235 * \boldsymbol{t} = SSA \tag{2}$$

For each simulation, the error in predicting the training data set and the test data point was calculated and plotted (**Figure 6**). The data points lying above (below) the line indicate that the linear regression predictive model has overpredicted (underpredicted) the SSA. The best line fit for the data points is generated and the R^2 is calculated which indicates the goodness of fit of the predictive model on the training data. When incorporating time to the model, the average error lowers to 12.9% and the R^2 coefficient is 0.34 (Table 2). This is a marked improvement from using temperature data alone and the results better describe the SSA variation occurring over a temperature differential of 50°C. However, the model is not accurate over all data points even though the average error is low as shown in **Figure 6**. In other words, the model is accurate for some but not all the data. This discrepancy can be quantified using the R^2 value, indicating the amount of data variability in the model, with roughly a 3x increase from the temperature-only model which had a value of 0.12.

Table 2. Comparison of model statistics across all reported SSA models.

Parameters of Interest	Percent Error		R^2 Coefficient	
	Average	Standard Deviation	Average	Standard Deviation
Calcination Parameters Only (T & t)	12.90%	9.3002	0.3437	0.0356
Precipitation Parameters Only (M & C)	10.65%	7.8573	0.3236	0.0491
Precipitation & Calcination Parameters (T, t, M & C)	8.41%	5.0744	0.7376	0.0151

Our next model follows the same LOO methodology but evaluates how the nitric acid and plutonium concentrations affected the SSA without inclusion of calcination conditions. Equation 3 shows the form with the average coefficients across the simulation runs are 0.03231 and 0.2332 for A_3 and A_4, respectively. Of the two coefficients, there is larger variability with A_3 suggesting the data are not representative of the nitric acid concentration effect. However, the model performed better than evaluating calcination temperature alone and had a lower average prediction error and R^2 value of 10% and 0.32, respectively (Table 2).

$$0.03231 * \boldsymbol{M} + 0.2332 * \boldsymbol{C} = SSA \qquad (3)$$

These results were unexpected since precipitation parameters alone have not been attributed to affecting the PuO$_2$ SSA. From **Figure 6** and Table 2, Equation 3 results in lower values for average error and statistically the same R^2 coefficient when compared to Equation 2. Comparison of the experimental and predicted SSA (**Figure 6**) shows two distinct clustering of values at ~7 m^2/g and again ~9.5 m^2/g. During the middle of the campaign, an effort was made to increase the Pu concentration from ~30 g/L to ~45 g/L, and in general, higher SSAs were seen with higher Pu concentration. Although there was some variation in the nitric acid concentration early on (**Figure 2**), the concentration remained steady at 2.6 M, well within industrial-scale processing parameters. While the results are interesting, the model is only capturing about 32% of the data variability and therefore very limited in its predictive capabilities.

The last model defined in Equation 4 describes the specific form of this four-parameter model for the prediction of SSA. An important note is that the value of the A_3 coefficient, which corresponds to the nitric acid molarity parameter, has a similar value to the linear regression in **Figure 2**, corroborating the preliminary hypothesis of a negative correlation between the nitric acid molarity and SSA. Also, the coefficient is stabilized with respect to the average value and sign. The average error and R^2 value in the prediction of SSA were found to be 8.41% and 0.74, respectively. Interestingly, results from simulation 15 show that most of the data now reside to ~10% error compared to experiment (**Figure 6**). Also, while the model improves the predictability overall, simulation 21 is a significant outlier. When the process parameters of the test data point associated with simulation 21 were compared to the training data set, the nitric acid molarity was outside the training model range and hence the predicted value must be extrapolated rather than interpolated. The error associated with simulation 21 shows that the regression model developed here is highly accurate for simulations involving interpolation of data while it is less accurate for simulations involving extrapolation. Therefore, our analysis is highly accurate for the given processing parameter range and can be extended to encompass the full range of processing parameters with more experimental data.

$$0.01162 * T - 0.0013 * t - 1.7299 * M + 0.15604 * C = SSA \qquad (4)$$

While a direct comparison of the parameter coefficients across all three models would be desired, it is often not possible due to the nature of regression modeling wherein the coefficient values are defined by the data that is chosen as the training dataset. However, an indirect comparison of the coefficient signs can provide insight into the trends of the data. For example, in Equation 2 and Equation 4 the calcination temperature coefficient is positive while the calcination time coefficient is negative. Therefore, the trend shows that SSA tends to increase with an increase in temperature but decrease with an increase in time. This is a counter description to the known correlations of increasing calcination temperature leading to decreases in the SSA, but instead is reflective of the dataset used to generate the model. **Figure 4** compares the calcination temperature with the SSA for all data points used from the SRS dataset and shows a positive trend with increasing temperature corresponding to an increase in SSA.
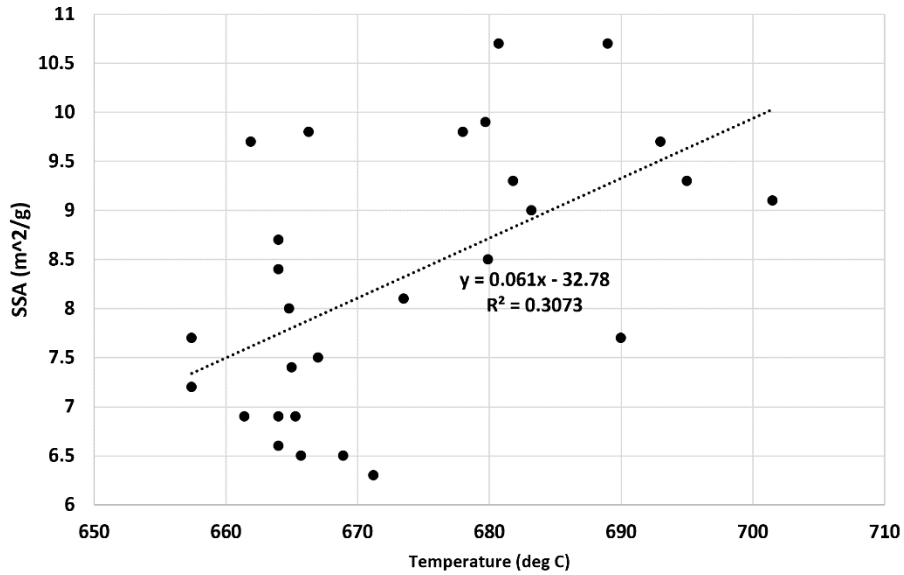

Figure 4: Comparison of SSA and Calcination Temperature across the SRS dataset.

This trend is believed to be artificial as the data points were obtained from samples calcined in two different furnaces. The first furnace at low temperature was calcined for almost twice the time that the high temperature furnace was held at temperature. Therefore, this positive trend in the temperature can actually be associated with the hold time parameter. As such it is expected that with a larger dataset the accepted decreasing trend with increasing temperature will be identified by the model. Furthermore, in both Equation 3 and Equation 4 the Pu(IV) nitrate concentration coefficient is positive while the nitric acid concentration coefficient fluctuates between positive to negative values, predicting the SSA tends to increase with increasing Pu(IV) nitrate concentration.

However, the same conclusion cannot be gathered from the nitric acid concentration. This could be due to the lack of data available as the nitric acid concentration values were obtained for only a relatively small range. The scatter of the residuals from Equation 4 versus the predicted SSA (**Figure 5**) illustrates that a simple model achieves moderately high accuracy in terms of R^2. The scatter of the residuals is random, indicating no ties in the data. Moreover, the random underprediction and overprediction i.e., data points lying randomly under and over the identity line, indicate that the model is not biased in a certain direction. Comparison of the R^2 for the three predictive models reveals that including precipitation parameters and calcination time to the general correlations of temperature has the best estimation power. Thus, inclusion of the precipitation parameters may be preferred for the predictive modeling of the PuO_2 SSA. This is a significant revelation for industrial-scale PuO_2 process optimization to reduce the SSA within tight controls defined by the facility requirements.
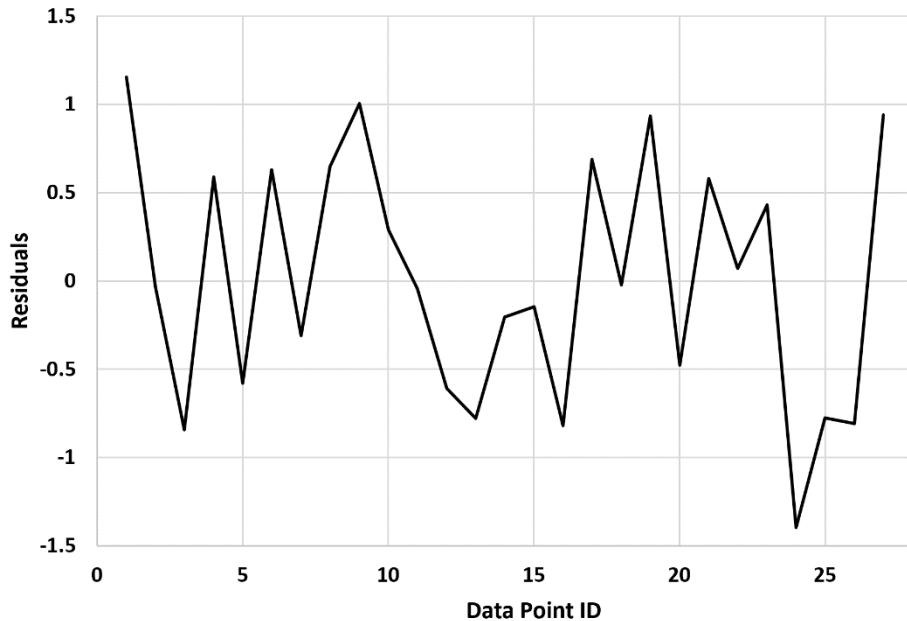

Figure 5: Plot of residuals for each data point using Equation 4 to fit the data.
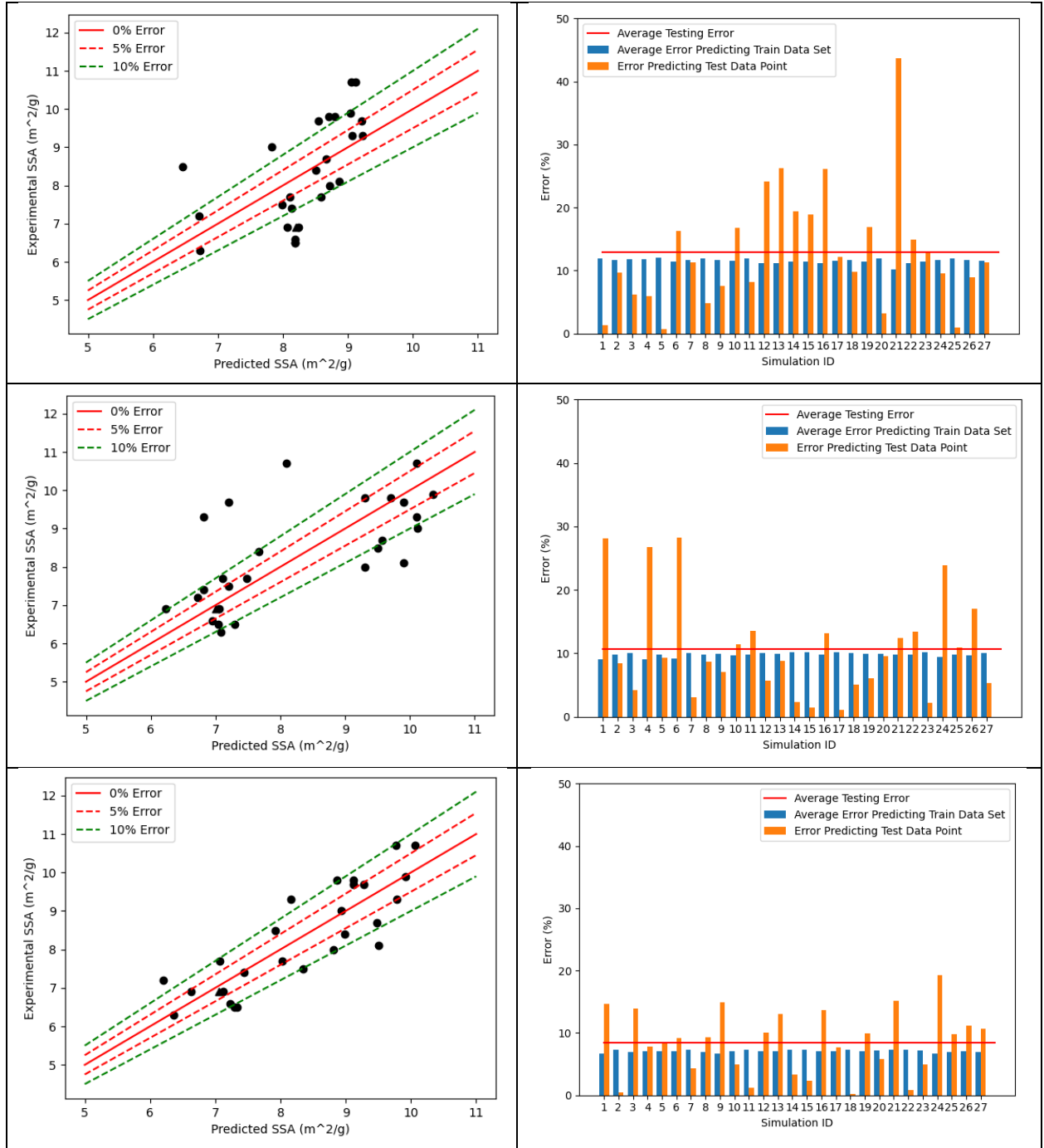
Figure 6: Comparison of the predicted vs experimentally measured SSA (left) and the corresponding calculated errors (right) for all simulations showing lines of 5% and 10% error for simulation #15. Top results illustrate the model evaluating calcination parameters only, middle for precipitation parameters only, and bottom for both calcination and precipitation parameters.

Conclusions

Multiple linear regression models based on precipitation and calcination parameters were developed to predict the SSA from the PuO_2 production data, specifically the target nitric acid and Pu(IV) nitrate concentrations during precipitation, and the calcination temperature and time. Our analysis showed that individual unit operations (e.g. only calcination or precipitation parameters) have an average error similar to the conventional temperature-only model but a nearly three-times increase in the description of the variability of the data. However, the final model which utilized both precipitation parameters and calcination parameters to predict PuO_2 SSA was not only more accurate than the conventional model with a decrease in average error from 13.90% to 8.41%, but also showed an increase in the R^2 coefficient from 0.1202 to 0.7376, thereby showing both precipitation and calcination provides the best predictive capability out of the models shown here. Therefore, inclusion of precipitation parameters to a calcination time-temperature model could allow for more accurate prediction of the PuO_2 SSA, which has not been identified by previous studies. Furthermore, although data are limited, an exhaustive analysis of all possible process parameter combinations may be needed to identify further parameters of interest, for example, oxalate concentration, impurity concentration and carbon content. This justifies the need for advanced machine learning algorithms to provide model comparisons to quantify the model predictive capabilities as a function of process parameters.

Supplementary Information

Discussion on the regression analyses of PuO_2 SSA vs. calcination temperature, coefficient values for each question across all 27 simulations performed.

Acknowledgements

Author Information

The authors can be reached at eric.hoar@srnl.doe.gov for Eric Hoar, lindsay.roy@srnl.doe.gov for Lindsay Roy and thomas.shehee@srnl.doe.gov for Thomas Shehee.

References

(1)   Orr, R. M.; Sims, H. E.; Taylor, R. J. A review of plutonium oxalate decomposition reactions and effects of decomposition temperature on the surface area of the plutonium dioxide product. *J. Nucl. Mater.* **2015**, *465*, 756-773.

(2)   Daniel, G. *Literature Review of PuO2 Calcination Time and Temperature Data for Specific Surface Area*, *SRNL-TR-2011-00334*; Savannah River National Laboratory: Aiken, SC, 2012.

(3)   Greintz, R. M.; Neal, D. H. *Plutonium(IV) oxalate precipitation and calcination process for plutonium nitrate to oxide conversion*; Rocky Flats Plant: Golden, CO, 1978.

(4)   Machuron-Mandard, X.; Madic, C. Plutonium dioxide particle properties as a function of calcination temperature. *J. Alloys Compd.* **1996**, *235*, 216-224.

(5)   Alwin, J. L.; Coriz, F.; Danis, J. A.; Bluhm, B. K.; Wayne, D. W.; Gray, D. W.; Ramsey, K. B.; Costa, D. A.; Bluhm, E. A.; Nixon, A. E.; Garcia, D. J.; Roybal, J. D.; Saba, M. T.; Valdez, J. A.; Martinez, D.; Martinez, J. R.; Martinez, C. M.; Martinez, Y. A.; Martinez, C. M. Plutonium oxide polishing for MOX fuel fabrication. *J. Alloys Compd.* **2007**, *444-445*, 565-568.

(6)   Bluhm, E. A.; Abney, K. D.; Balkey, S.; Brock, J. C.; Coriz, F.; Dyke, J. T.; Garcia, D. J.; Griego, B. J.; Martinez, B. T.; Martinez, D.; Martinez, J. R.; Martinez, Y. A.; Morgan, L.; Roybal, J. D.; Valdez, J. A.; Ramsey, K. B.; Bluhm, B. K.; Martinez, C. D.; Valdez, M. M. Plutonium Oxide Polishing for MOX Fuel Production. *Sep. Sci. Technol.* **2005**, *40*, 281-296.

(7)   Wayne, D. M.; Peppers, L. G.; Schwartz, D. S.; DeBurgomaster, P. C. Surface area and particle size distribution of plutonium oxides derived from the direct oxidation of Pu metal. *J. Nucl. Mater.* **2018**, *511*, 242-263.

(8)   Smith, P. K.; Burney, G. A.; Rankin, D. T.; Bickford, D. F.; Sisson, J., R D: Effect of oxalate precipitation on PuO2 microstructures. In *Conference: 6. international symposium - ceramic microstructures 176, Berkeley, CA, USA, 24 Aug 1976*: United States, 1976; pp Medium: ED; Size: Pages: 11.

(9)   Crowder, M. L.; Duffey, J. M.; Livingston, R. R.; Scogin, J. H.; Kessinger, G. F.; Almond, P. M. Moisture and surface area measurements of plutonium-bearing oxides. *J. Alloys Compd.* **2009**, *488*, 565-567.

(10)   Hill, B. C. *Effect of Precipitation Conditions on the Specific Surface Area of Neptunium Oxide*, *WSRC-TR-2004-00296*; Savannah River Site: Aiken, SC, 2004.

(11)   Fan, C.; Xiao, F.; Yan, C.; Liu, C.; Li, Z.; Wang, J. A novel methodology to explain and evaluate data-driven building energy performance models based on interpretable machine learning. *Appl. Energy* **2019**, *235*, 1551-1560.

(12)   McCoy, J. T.; Auret, L. Machine learning applications in minerals processing: A review. *Miner. Eng.* **2019**, *132*, 95-109.

(13)   von Stosch, M.; Oliveira, R.; Peres, J.; Feyo de Azevedo, S. Hybrid semi-parametric modeling in process systems engineering: Past, present and future. *Comput. Chem. Eng.* **2014**, *60*, 86-101.

(14)   Zhou, Q.; Lu, S.; Wu, Y.; Wang, J. Property-Oriented Material Design Based on a Data-Driven Machine Learning Technique. *J. Phys. Chem. Lett.* **2020**, *11*, 3920-3927.

(15)   Crowder, M.; Pierce, R. *Lab-Scale Demonstration of Plutonium Purification by Anion Exchange, Plutonium(IV) Oxalate Precipitation, and Calcination to Plutonium Oxide to Support the MOX Feed Mission*; Savannah River National Laboratory: Aiken, SC, 2012.

(16)   Crowder, M.; Pierce, R.; Scogin, J.; Daniel, G.; King, W. *Small-Scale Testing of Plutonium(IV) Oxalate Precipitation and Calcination to Plutonium Oxide to Support the MOX Feed Mission*; Savannah River National Laboratory: Aiken, SC, 2012.

(17)   Zhang, L.; Sun, B.; Zhang, Q.; Liu, H.; Liu, K.; Song, H. The adsorption thermodynamics of H2O and CO2 on PuO2(1 1 1) surface: A comparative study based on DFT+U-D3. *Appl. Surf. Sci.* **2021**, *537*, 147882.

(18)   Pegg, J. T.; Shields, A. E.; Storr, M. T.; Scanlon, D. O.; de Leeuw, N. H. Interaction of hydrogen with actinide dioxide surfaces. *J. Chem. Phys.* **2020**, *153*, 014705.

(19)   Farr, J. D.; Schulze, R. K.; Neu, M. P. Surface chemistry of Pu oxides. *J. Nucl. Mater.* **2004**, *328*, 124-136.

(20)   Jomard, G.; Bottin, F.; Geneste, G. Water adsorption and dissociation on the PuO2(1 1 0) surface. *J. Nucl. Mater.* **2014**, *451*, 28-34.

(21)   Sun, B.; Liu, H.; Song, H.; Zhang, G.; Zheng, H.; Zhao, X.; Zhang, P. First-principles study of surface properties of PuO2: Effects of thickness and O-vacancy on surface stability and chemical activity. *J. Nucl. Mater.* **2012**, *426*, 139-147.

(22)   Pegg, J. T.; Shields, A. E.; Storr, M. T.; Scanlon, D. O.; de Leeuw, N. H. Noncollinear Relativistic DFT + U Calculations of Actinide Dioxide Surfaces. *J. Phys. Chem. C* **2019**, *123*, 356-366.

(23)   Wellington, J. P. W.; Tegner, B. E.; Collard, J.; Kerridge, A.; Kaltsoyannis, N. Oxygen Vacancy Formation and Water Adsorption on Reduced AnO2{111}, {110}, and {100} Surfaces (An = U, Pu): A Computational Study. *J. Phys. Chem. C* **2018**, *122*, 7149-7165.

(24)   Nelson, A. J.; Holliday, K. S.; Stanford, J. A.; Grant, W. K.; Erler, R. G.; Allen, P.; McLean, W.; Roussel, P. Adsorption of atmospheric gases on Pu surfaces. *MRS Online Proc. Libr.* **2012**, *1444*.

(25)   Jomard, G.; Bottin, F. Thermodynamic stability of PuO2 surfaces: Influence of electronic correlations. *Phys. Rev. B: Condens. Matter Mater. Phys.* **2011**, *84*, 195469/195461-195469/195468.

(26)   Venault, L.; Deroche, A.; Gaillard, J.; Lemaire, O.; Budanova, N.; Vermeulen, J.; Maurin, J.; Vigier, N.; Moisy, P. Dihydrogen H2 steady state in α-radiolysis of water adsorbed on PuO2 surface. *Radiat. Phys. Chem.* **2019**, *162*, 136-145.

(27)   George, N. I.; Bowyer, J. F.; Crabtree, N. M.; Chang, C.-W. An Iterative Leave-One-Out Approach to Outlier Detection in RNA-Seq Data. *PLOS ONE* **2015**, *10*, e0125224.
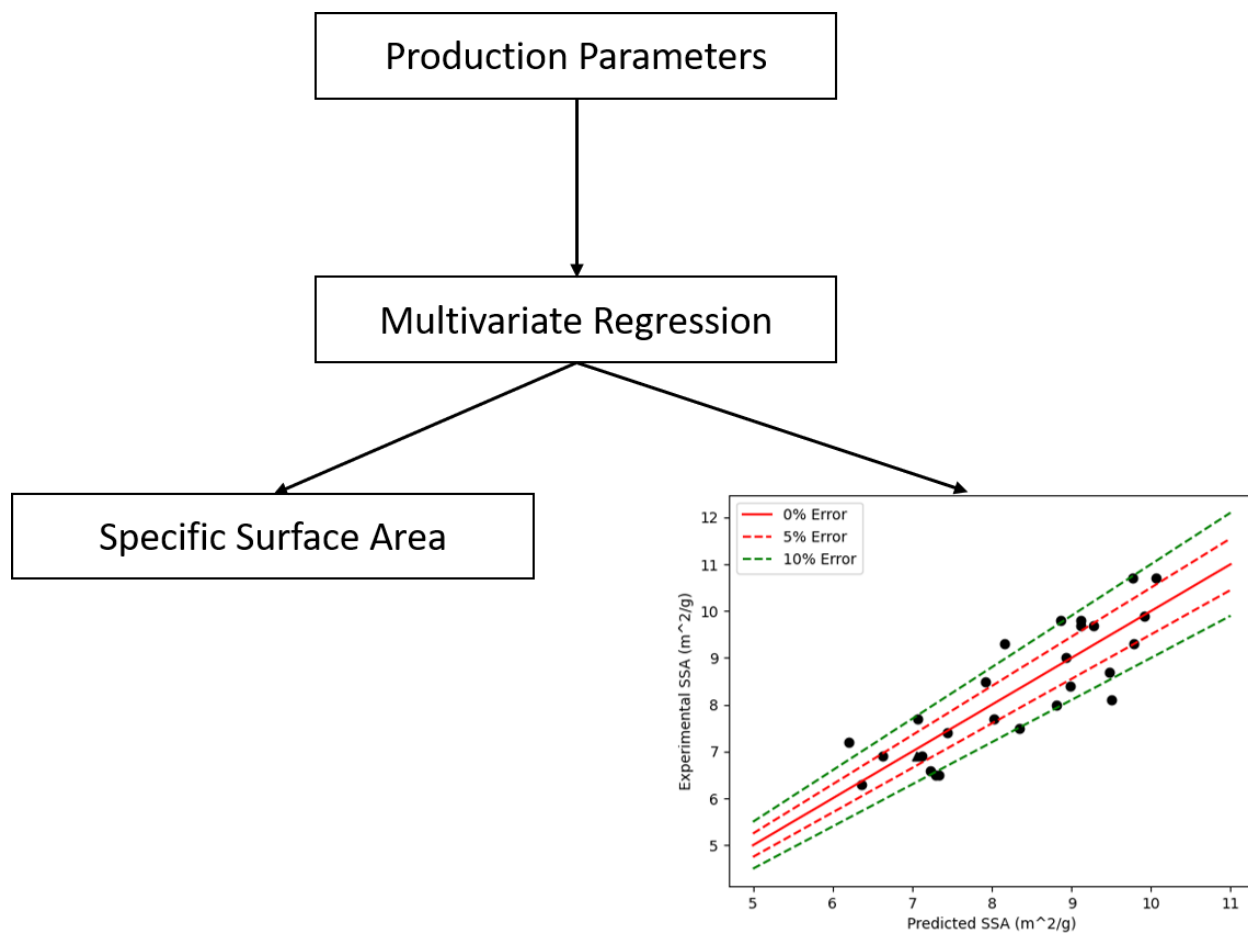
For Table of Contents Only

Impact of Precipitation Parameters on the Specific Surface Area of PuO$_2$ – Supplementary Material

Eric Hoar, Thomas C. Shehee and Lindsay E. Roy*

Contributions from Savannah River National Laboratory, P. O. Box A, Aiken, SC 29808

* To whom correspondence should be addressed (eric.hoar@srnl.doe.gov)

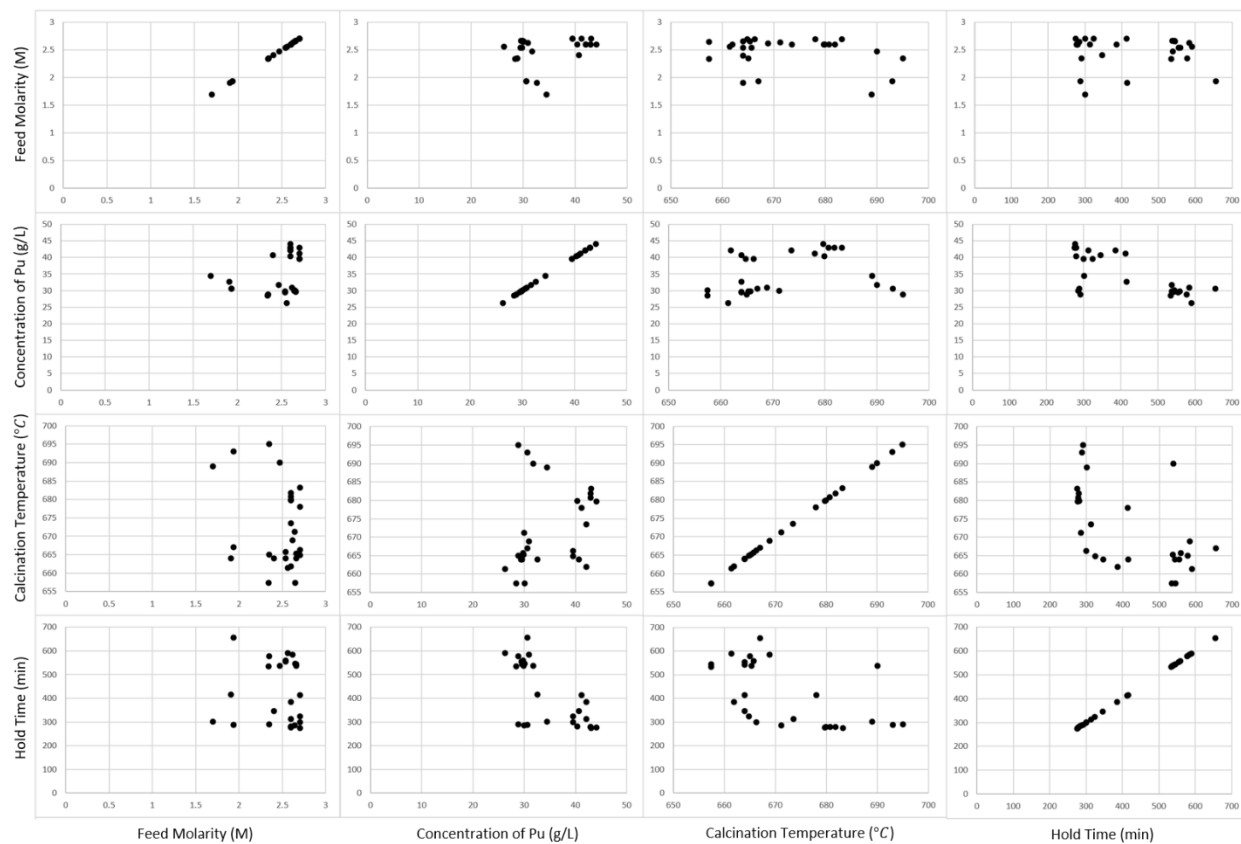# S1. Multicollinearity Analysis of Input Parameters

Figure S1: Plots describing the multicollinearity of the input parameters. The plots show that there is no multicollinearity in the input parameters.

S2. Analysis of the PuO₂ SSA with Temperature

Estimation of the approximate SSA vs calcination temperature is generally represented as an exponential function fitted to known experimental data. Equation S1 shows the generalized form of Equation 19 from Orr *et al.*[S1] which we trained using our SRS dataset.

$$e^{A_1 * T + A_2} = SSA \tag{S1}$$

While training Equation S1, the model remained non-converged for 1E9 iterations, near the limit of our current capabilities. Therefore, the constant term was removed to form Equation S2 and the model was retrained using the iterative leave-one-out (LOO) methodology utilized throughout our analysis.

$$e^{A_1 * T} = SSA \tag{S2}$$

Table S1 specifies the value of the A_1 coefficient obtained for each simulation in the LOO methodology as well as the average coefficient value and the standard deviation. Furthermore, Figure S2 compares the calculated errors for all simulations performed and Figure S3 compares the predicted and measured SSA for simulation #15 using Equation S2. The average error associated with Equation S2 is 13.66% and the average R^2 value was calculated as 0.1686.

Table S1: Values of the A1 coefficient for equation S2 (Orr's Equation without Constant) across all 27 simulations performed using the leave one out methodology.

Simulation ID	A_1 for SSA Prediction
1	0.003156
2	0.003164
3	0.003163
4	0.003153
5	0.003157
6	0.003144
7	0.003167
8	0.003160
9	0.003153
10	0.003166
11	0.003173
12	0.003169
13	0.003170
14	0.003167
15	0.003167

16	0.003171
17	0.003149
18	0.003149
19	0.003143
20	0.003154
21	0.003159
22	0.003156
23	0.003148
24	0.003161
25	0.003155
26	0.003160
27	0.003148
Average:	0.003156
Standard Deviation:	8.3487E-06

Figure S2: Comparison of calculated errors for all simulations performed using Equation S2 to predict SSA.

Figure S3: Comparison of the predicted vs measured SSA for simulation #15 using Equation S2, showing lines of 5% and 10% error.

Based on the plot of SSA vs. calcination temperature in **Figure 1** of the main text, the SRS data were evaluated using a linear model since an exponential decrease was not observed over the narrow temperature range. The model utilized Equation S3 with the calculated errors for each simulation plotted in Figure S4 and comparison between the predicted vs. measured SSA for simulation #15 plotted in Figure S5.

$$A_1 * T = SSA \tag{S3}$$

Table S2 describes the values of the trained A_1 coefficient for Equation S3. An average coefficient value of 0.012403 produced an average prediction error and R^2 value of 13.9% and 0.12024, respectively. Using Equation S3, the average SSA over the data is calculated to be 8.292 ± 0.29 m^2/g. For comparison, Equation S2 predicts an average SSA of 8.285 ± 0.55 m^2/g over the range.

When their performaces are compared, the average error was found to be approximately the same and the average R^2 decreased to 0.12 for Equation S3 from 0.17 for Equation S2. However, this is not a significant increase in our model's predictive capability and an exponential dependency of the PuO_2 SSA with calcination temperature has no physical meaning. Therefore, it was concluded that for our SRS dataset, a linear model for the prediction of SSA from temperature was sufficient.
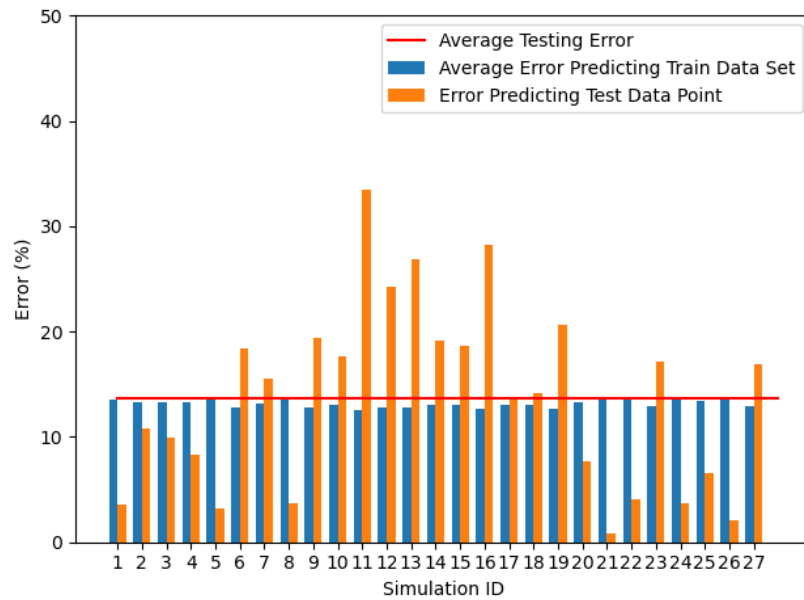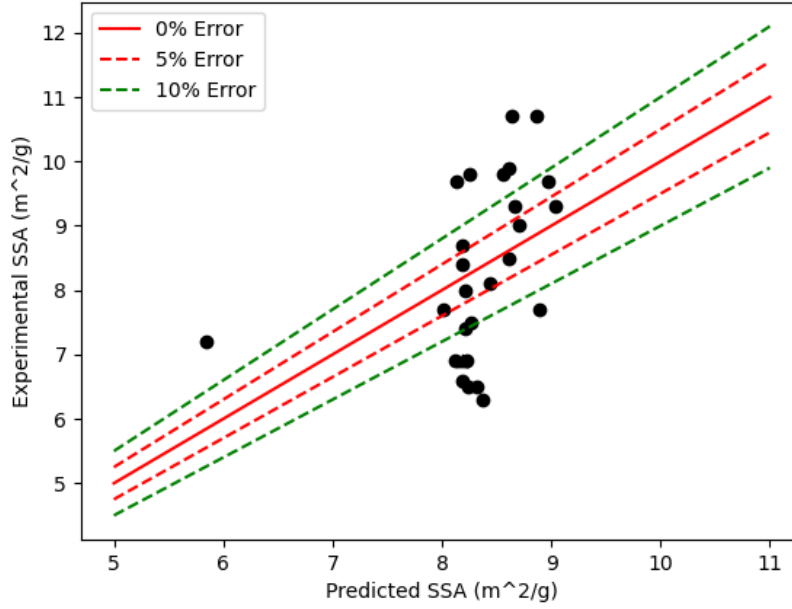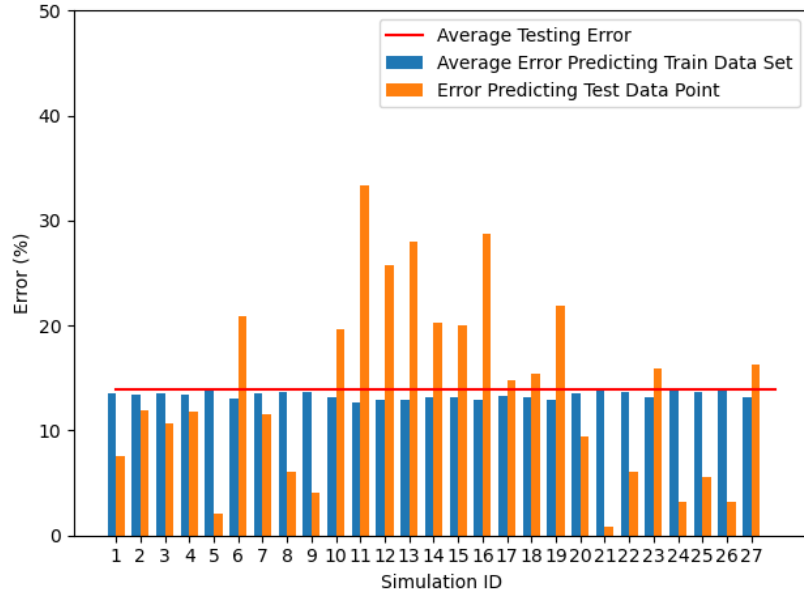
Figure S4: Comparison of calculated errors for all simulations performed using Equation S3 to predict SSA.
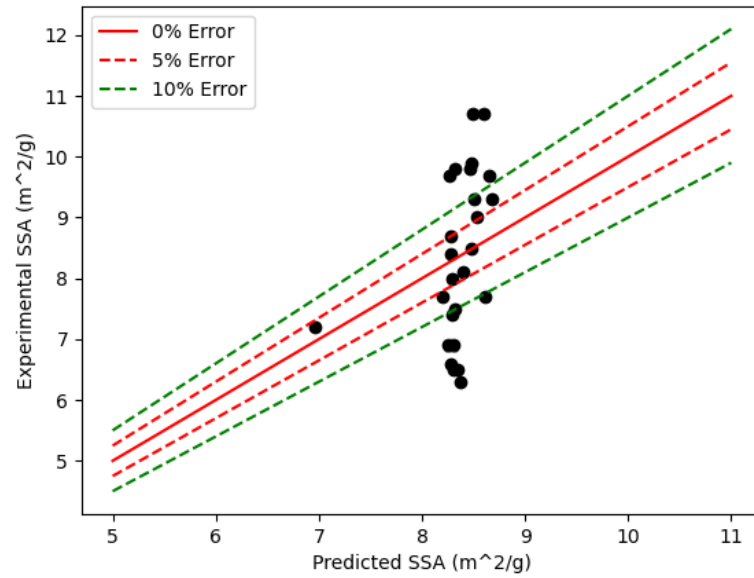

Figure S5: Comparison of the predicted vs. measured SSA for simulation #15 using Equation S3, showing lines of 5% and 10% error.

Table S2: Values of the A_1 coefficient for equation S3 across all 27 simulations performed using the leave one out methodology.

Simulation ID	A_1 for SSA Prediction
1	0.012362
2	0.012451

3	0.012447
4	0.012337
5	0.012393
6	0.012275
7	0.012454
8	0.012428
9	0.012389
10	0.012477
11	0.01252
12	0.012496
13	0.012503
14	0.01248
15	0.012479
16	0.012506
17	0.012322
18	0.012317
19	0.012271
20	0.012353
21	0.012399
22	0.012372
23	0.012318
24	0.012417
25	0.012376
26	0.012417
27	0.012315
Average:	0.012403
Standard Deviation:	7.2365E-05

S3. Calculated Coefficients Across All Simulations

Table S3: Values of the A_1 and A_2 coefficients for equation 2 (Calcination Parameters Only) across all 27 simulations performed using the leave one out methodology.

Simulation ID	A_1 for SSA Prediction	A_2 for SSA Prediction
1	0.014168	-0.00231
2	0.014208	-0.0023
3	0.014187	-0.00229
4	0.014099	-0.00225
5	0.014193	-0.00233
6	0.013933	-0.00212

7	0.014234	-0.00232
8	0.014202	-0.00232
9	0.014185	-0.00236
10	0.014213	-0.00228
11	0.014071	-0.00214
12	0.014247	-0.00229
13	0.014249	-0.00228
14	0.014247	-0.00231
15	0.014242	-0.0023
16	0.014234	-0.00226
17	0.01407	-0.00226
18	0.01404	-0.00221
19	0.013912	-0.0021
20	0.014142	-0.00229
21	0.015257	-0.00399
22	0.014269	-0.00253
23	0.014058	-0.00225
24	0.014292	-0.00241
25	0.014177	-0.00232
26	0.014279	-0.00239
27	0.014034	-0.00221
Average:	0.014202	-0.00235
Standard Deviation:	0.00023	0.00033

Table S4: Values of the A_3 and A_4 coefficients for equation 3 (Precipitation Parameters Only) across all 27 simulations performed using the leave one out methodology.

Simulation ID	A_3 for SSA Prediction	A_4 for SSA Prediction
1	-0.16161	0.244385
2	-0.01428	0.235893
3	0.043682	0.232122
4	0.132003	0.223936
5	0.089625	0.228471
6	0.472288	0.199631
7	0.017989	0.233968
8	-0.048	0.238167
9	-0.00829	0.235576
10	-0.09178	0.241175

11	0.133045	0.226979
12	0.070949	0.230846
13	0.088909	0.229782
14	0.052034	0.231976
15	0.044694	0.23243
16	0.117895	0.228052
17	0.035047	0.232871
18	-0.0169	0.237269
19	0.082885	0.22887
20	-0.03908	0.23927
21	-0.01269	0.237584
22	-0.03946	0.239704
23	0.017299	0.234502
24	-0.09741	0.244604
25	-0.05267	0.240231
26	0.020544	0.235614
27	0.035646	0.232357
Average:	0.03231	0.233195
Standard Deviation:	0.11136	0.00832

Table S5: All coefficient values for equation 4 (Precipitation & Calcination Parameters) across all 27 simulations performed using the leave one out methodology.

Simulation ID	A_1 for SSA Prediction	A_2 for SSA Prediction	A_3 for SSA Prediction	A_4 for SSA Prediction
1	0.010666	-0.00104	-1.73425	0.169789
2	0.011641	-0.00126	-1.73726	0.156096
3	0.012552	-0.00112	-2.0075	0.1567
4	0.010747	-0.0012	-1.56178	0.159063
5	0.012238	-0.00125	-1.91131	0.15746
6	0.010365	-0.00126	-1.35276	0.152227
7	0.011736	-0.00127	-1.73696	0.154675
8	0.01168	-0.00123	-1.84542	0.16172
9	0.011977	-0.00127	-1.88359	0.159181
10	0.011551	-0.00125	-1.77989	0.160268
11	0.011617	-0.00124	-1.73578	0.156127
12	0.01172	-0.00128	-1.67765	0.151325
13	0.011742	-0.00128	-1.66692	0.150349
14	0.011622	-0.00128	-1.70286	0.154442

15	0.011623	-0.00127	-1.71233	0.154958
16	0.011629	-0.00128	-1.64291	0.150767
17	0.011949	-0.00123	-1.78798	0.152386
18	0.011616	-0.00127	-1.73665	0.156564
19	0.011965	-0.00116	-1.75546	0.148465
20	0.011457	-0.00132	-1.72825	0.160343
21	0.012254	-0.00195	-1.55308	0.140014
22	0.01167	-0.00128	-1.735	0.155498
23	0.011839	-0.00125	-1.75269	0.152582
24	0.011092	-0.00139	-1.69054	0.166895
25	0.011541	-0.0013	-1.78384	0.162674
26	0.011238	-0.00136	-1.63317	0.158853
27	0.012063	-0.00113	-1.86049	0.153623
Average:	0.011622	-0.00128	-1.72986	0.156039
Standard Deviation:	0.00047	0.00015	0.12204	0.00577

References

(S1)   Orr, R. M.; Sims, H. E.; Taylor, R. J. A review of plutonium oxalate decomposition reactions and effects of decomposition temperature on the surface area of the plutonium dioxide product. *J. Nucl. Mater.* **2015**, *465*, 756-773.